AGU PUBLICATIONS

Geochemistry, Geophysics, Geosystems

RESEARCH ARTICLE
10.1002/2015GC006041

Key Points:
- Carbonate veins record fluid flow through an oceanic core complex footwall
- Carbonate precipitation is strongly correlated with nonserpentinized olivine
- Distinct carbonate vein generations record variations fluid flow and mixing

Supporting Information:
- Supporting Information S1
- Data Set S1
- Data Set S2
- Data Set S3
- Data Set S4

Correspondence to:
T. Schroeder,
tschroeder@bennington.edu

Citation:
Schroeder, T., W. Bach, N. Jöns, S. Jöns, P. Monien, and A. Klügel (2015), Fluid circulation and carbonate vein precipitation in the footwall of an oceanic core complex, Ocean Drilling Program Site 175, Mid-Atlantic Ridge, *Geochem. Geophys. Geosyst.*, *16*, 3716–3732, doi:10.1002/2015GC006041.

Received 5 AUG 2015
Accepted 8 OCT 2015
Accepted article online 13 OCT 2015
Published online 30 OCT 2015

Fluid circulation and carbonate vein precipitation in the footwall of an oceanic core complex, Ocean Drilling Program Site 175, Mid-Atlantic Ridge

Tim Schroeder[1], Wolfgang Bach[2,3], Niels Jöns[2,3,4], Svenja Jöns[2,4], Patrick Monien[2], and Andreas Klügel[2]

[1]Natural Sciences Division, Bennington College, Bennington, Vermont, USA, [2]Department of Geosciences, University of Bremen, Bremen, Germany, [3]MARUM Center for Marine Environmental Geosciences, Bremen, Germany, [4]Now at Institut für Geologie, Mineralogie und Geophysik, Ruhr Universität Bochum, Bochum, Germany

Abstract Carbonate veins recovered from the mafic/ultramafic footwall of an oceanic detachment fault on the Mid-Atlantic Ridge record multiple episodes of fluid movement through the detachment and secondary faults. High-temperature (~75–175°C) calcite veins with elevated REE contents and strong positive Eu-anomalies record the mixing of up-welling hydrothermal fluids with infiltrating seawater. Carbonate precipitation is most prominent in olivine-rich troctolite, which also display a much higher degree of greenschist and sub-greenschist alteration relative to gabbro and diabase. Low-temperature calcite and aragonite veins likely precipitated from oxidizing seawater that infiltrated the detachment fault and/or within secondary faults late or post footwall denudation. Oxygen and carbon isotopes lie on a mixing line between seawater and Logatchev-like hydrothermal fluids, but precipitation temperatures are cooler than would be expected for isenthalpic mixing, suggesting conductive cooling during upward flow. There is no depth dependence of vein precipitation temperature, indicating effective cooling of the footwall via seawater infiltration through fault zones. One sample contains textural evidence of low-temperature, seawater-signature veins being cut by high-temperature, hydrothermal-signature veins. This indicates temporal variability in the fluid mixing, possibly caused by deformation-induced porosity changes or dike intrusion. The strong correlation between carbonate precipitation and olivine-rich troctolites suggests that the presence of unaltered olivine is a key requirement for carbonate precipitation from seawater and hydrothermal fluids. Our results also suggest that calcite-talc alteration of troctolites may be a more efficient CO_2 trap than serpentinized peridotite.

1. Introduction

Seawater circulation and water-rock interaction on the flanks of mid-ocean ridges affect the composition, structure, and geophysical signature of oceanic lithosphere as well as the composition of seawater [*Mottl and Wheat*, 1994; *Elderfield and Schultz*, 1996; *Wheat and Mottl*, 2000; *Alt and Teagle*, 2003; *Bach et al*., 2003; *Teagle et al*., 2003; *Coggon et al*., 2004, 2010]. This process has been much better documented in "normal" volcanically constructed oceanic lithosphere than in the tectonically denuded lower crust and upper mantle rocks found on the flanks of nonvolcanic mid-ocean ridges [e.g., *Bach et al*., 2001, 2004]. The rugged topography, abundant faulting, and tectonic juxtaposition of diverse lithologies at nonvolcanic ridges cause more diversity in the nature of seawater-rock interaction than at volcanic ridges. Nonvolcanic ridges accommodate plate separation alternately via extensional faulting (including large displacement detachment faulting), and magmatic construction [*Cannat*, 1993; *Tucholke and Lin*, 1994; *Cann et al*., 1997; *Buck et al*., 2005; *Tucholke et al*., 2008]. Carbonate veins may record the infiltration of seawater and its evolution as a hydrothermal fluid at a wide range of sub-greenschist facies conditions [*Bonatti et al*., 1980; *Coggon et al*., 2004; *Eickmann et al*., 2009; *Bach et al*., 2011], and can thus be used to track the history of seawater-rock interaction during tectonic denudation and alteration of lower-crustal and mantle rock.

We report on seawater-rock interaction as recorded by carbonate veins and replacive carbonate in a large section of tectonically denuded gabbro containing ultramafic enclaves on the Mid-Atlantic Ridge flank at Ocean Drilling Program (ODP) Site 1275 (Figure 1). This work follows that of *Bach et al*. [2011], which studied seawater infiltration at nearby ODP Sites 1271 and 1274, also drilled during ODP Leg 209.

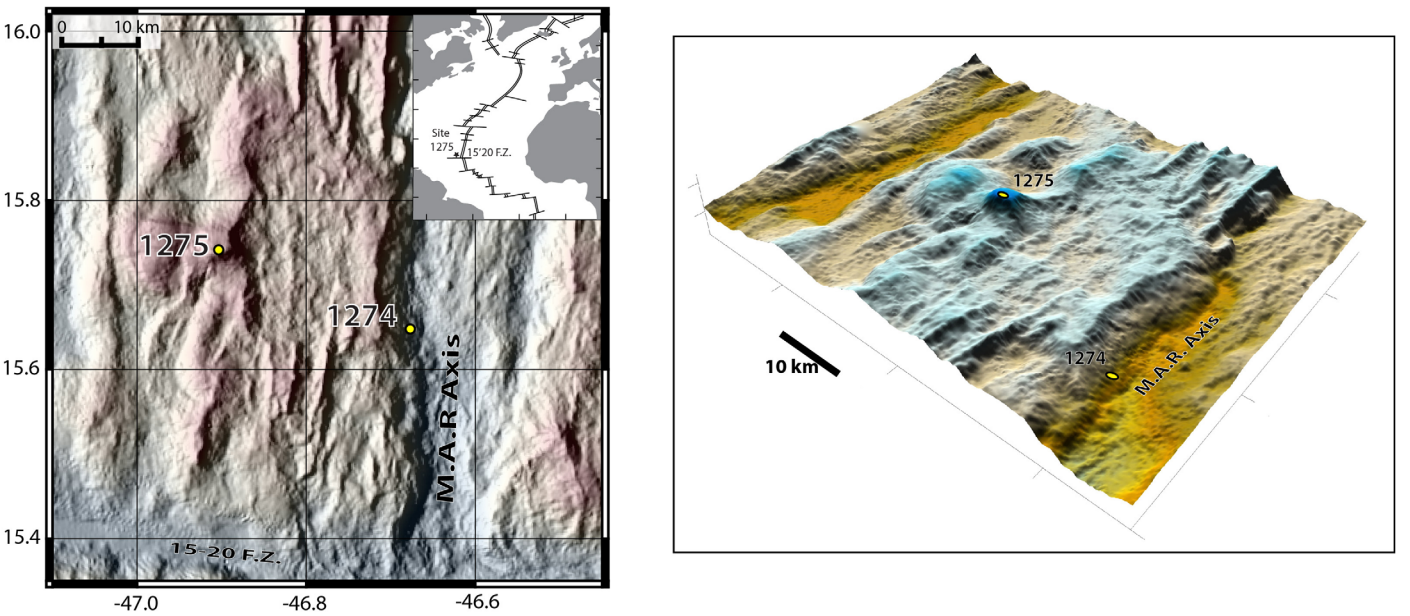

Figure 1. Map and perspective view showing location of ODP Site 1275 and surroundings.

Carbonation of olivine in ultramafic and mafic rocks has been proposed as an engineered reservoir for excess atmospheric CO_2 [*Kelemen and Matter*, 2008; *Power et al*., 2013]. This study documents that carbonate precipitation can occur under a wide range of conditions in this tectonic setting. Additionally, we document direct replacement of olivine by carbonate (carbonation) and the conditions under which it occurred.

2. Geologic Setting and Prior Work

Bach et al. [2011] documented multiple generations of carbonate veins at ODP Sites 1271 and 1274. High-temperature calcite veins at Site 1271 precipitated syntectonically and have oxygen isotopes that indicate precipitation temperatures of 90–170°C. However, strontium and lithium isotopes suggest fluid-rock interaction at much higher temperatures (300–400°C), and carbon isotopes suggest methanogenesis during high-temperature fluid-rock interaction. *Bach et al*. [2011] suggest that the temperature discrepancy between the temperature of rock interaction and precipitation from the fluid is due to conductive cooling during slow upward fluid migration. Aragonite veins precipitated at low temperatures at both Sites 1271 and 1274, likely after denudation of the seafloor surface. Carbonate precipitation at higher temperatures (indicated by oxygen isotopes) at greater depths in the holes suggest a geothermal gradient in the holes of 100–150°C km^{-1} at the time of vein precipitation [*Bach et al*., 2011].

Site 1271 core consists dominantly of mantle peridotite with small (<10 m wide) gabbro intrusions. There is evidence at Site 1271 for long-lived detachment faulting initiating at amphibolite facies conditions and continuing to sub-greenschist facies conditions near the seafloor [*Kelemen et al*., 2004; *Schroeder et al*., 2007]. The high-temperature calcite veins at Site 1271 are likely formed within this detachment fault zone. Site 1274 was drilled into a planar fault that dips beneath the axial valley and has approximately 3 km of displacement. Site 1274 core consists almost entirely of mantle peridotite, including incompletely and completely serpentinized harzburgite. There is no evidence for high-temperature or long-lived faulting in 1274 core, but abundant evidence for low-temperature faulting, including several zones of the partially cohesive fault gouge that are up to several meters wide [*Schroeder et al*., 2007].

The gabbro and troctolite that hosts veins at Site 1275 differs greatly from the Sites 1271 and 1274. Two successful holes were drilled at ODP Site 1275 to depths of 108.7 mbsf (Hole B) and 209.0 mbsf (Hole D) (Figure 2) into the eastern edge of a distinctly corrugated, flat-topped massif 35 km north or the 15°20′ Fracture Zone and 30 km west of the MAR axis [*Kelemen et al*., 2004, Figure 1]. The massif has been termed the "15°45′ Core Complex" by prior researchers, and is composed dominantly of gabbro, serpentinized

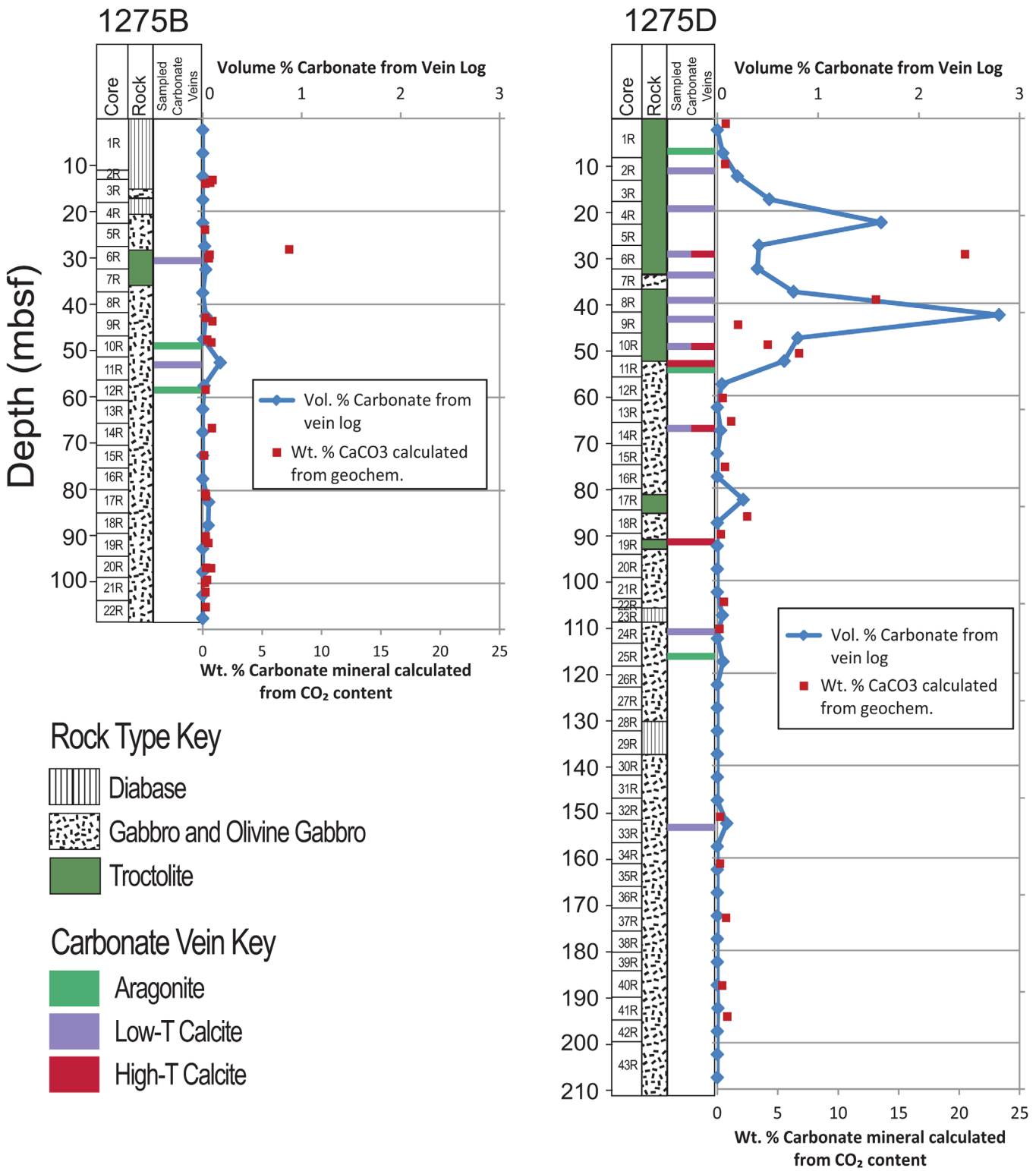

Figure 2. ODP Site 1275 down-hole plots showing dominant recovered lithology and the sample locations of the veins used in this study. Carbonate vein density (blue line) is calculated by the volume fraction of recovered core represented by carbonate veins (based on shipboard logs) binned in 5 m increments of curated depth; Red data points indicate the weight percent of shipboard geochemical samples that are carbonate based on analyzed CO_2 content.

peridotite, and small diabase intrusions that were exhumed along the detachment fault that caps the massif [*Macleod et al*., 2002; *Escartín et al*., 2003]. The Mid-Atlantic Ridge in this region (~50 km north and ~60 km south of the 15°20′ Fracture Zone) spreads by dominantly nonvolcanic processes, characterized by tectonic denudation of structurally deep rocks to the seafloor accompanied by limited shallow magmatic activity [*Schroeder et al*., 2007], and significant post-magnetization tectonic rotation of denuded basement [*Garcés and Gee*, 2007; *MacLeod et al*., 2011]. This region of nonvolcanic spreading includes several corrugated exposures that are likely oceanic core complexes capped by detachment faults [*Fujiwara et al*., 2003]. Much of the seafloor surface lacks volcanic constructional features; instead it is characterized by widely spaced, gently dipping smooth fault scarps [*Schroeder et al*., 2007]. Mantle peridotite is exposed on over 50% of the seafloor of the area [*Rona et al*., 1987; *Cannat et al*., 1997; *Escartín and Cannat*, 1999; *Fujiwara et al*., 2003].

ODP Site 1275 holes were drilled within 90 meters of each other on the eastern edge of the 15°45′ Core Complex; near an east-dipping (toward the ridge axis) steeper, secondary fault that cuts the detachment (Figure 1). This secondary fault likely formed after the denudation of the detachment footwall. The detachment fault and secondary faults provided multiple pathways for seawater infiltration into the core complex footwall. Recovered core consists dominantly of gabbro, oxide gabbro, olivine gabbro, and olivine-rich troctolite, with minor diabase [*Kelemen et al*., 2004]. Troctolites likely formed by the precipitation of clinopyroxene and plagioclase in dunite or olivine cumulate during interaction with migrating gabbroic melt [*Kelemen et al*., 2004].

In general, Site 1275 gabbros experienced a considerably lower degree of low-temperature alteration and veining than the troctolites. Gabbro alteration includes replacement of clinopyroxene by amphibole and minor chlorite, and replacement of plagioclase by secondary plagioclase and chlorite. Gabbro displays the highest degree of alteration in brittle deformation zones or near extensive fracture networks. Veins in gabbro largely consist of amphibole and chlorite, with more rare veins comprising combinations of zeolites, clay minerals, iron oxides, and carbonate. Troctolite includes abundant magmatic (gabbroic and some felsic) veins, near which olivine in the troctolite is replaced by talc, calcite, Fe-(oxy)hydroxides, serpentine and clays. Farther from magmatic veins, olivine is dominantly replaced by serpentinite and magnetite. Plagioclase near magmatic veins is replaced dominantly by clay minerals and calcite, while farther from magmatic veins it is replaced dominantly by secondary plagioclase and chlorite. Locally, vein mineralogy in troctolite is very similar to alteration mineralogy, and veins commonly grade in and out of mineral replacement textures. A more extensive description of alteration in Site 1275 core can be found in the Leg 209 Initial Reports volume [*Kelemen et al*., 2004].

3. Sample Description

We document at least five distinct types of carbonate mineralization in the Site 1275 core based on texture, mineralogy, and composition. These include replacive calcite, dolomite veins, early calcite veins, late calcite veins, and aragonite veins.

Replacive calcite, in association with talc, incompletely overprints olivine in several troctolite samples (Figure 3). Calcite precipitation may follow or be coeval with talc precipitation, but it is difficult to establish clear timing relationships between them. Some carbonated olivine grains are also partially replaced by celadonite, and some early calcite veins are partially filled by celadonite (Figure 3). Some zones of replacive calcite appear to grade into early calcite veins.

Early formed (established by cross-cutting relations) calcite veins appear in a wide variety of textures. Some consist of large (up to 0.5 mm diameter), equant grains that may contain inclusions of oxide, amphibole, and clay minerals (Figure 4a). Other early calcite veins are fine elongate or fibrous crystals oriented oblique or perpendicular to vein walls. Many early calcite veins also appear to be mechanically mixed or intergrown with talc, amphibole, and/or clay minerals, some of which are aligned to form a schistose fabric (Figures 4a and 4b). Some of these veins form phacoidal shear polyhedra with talc, and many early calcite veins contain crystals with deformation textures including mechanical twins, subgrains, and/or undulose extinction, indicating syn-tectonic emplacement. There appears to be a strong association between early calcite veins and talc veins, with some intergrowth between the two.

Dolomite veins may be the earliest episode of carbonate mineralization at Site 1275, but textural relations between dolomite veins and early calcite veins are not conclusive in all samples. Dolomite veins consist of

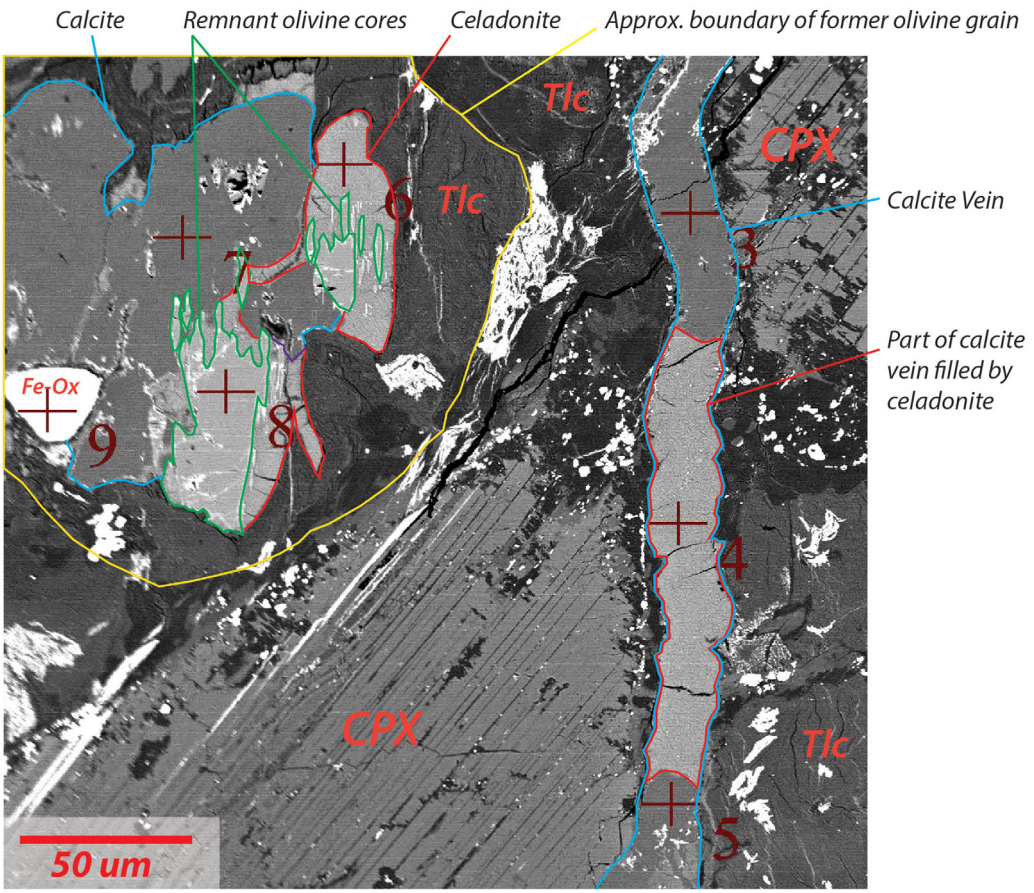

Figure 3. ODP Sample 1275 11R-2 6–10 cm–BSE micrograph of complex replacement textures on a former olivine grain and a calcite vein that is partially filled by celadonite in altered troctolite; the outer rim of the former olivine grain is replaced by talc with interspersed Fe-oxides; calcite and celadonite surround remnant olivine at the core of the grain; vein in the image is also filled alternately with calcite and celadonite.

large (up to 1 mm diameter), equant crystals that contain fine inclusions of Fe-oxides, or fine equant crystals in narrow veins. The crystals variably display undulose extinction, and where cut by microfaults, are recrystallized to more fine-grained aggregates. Dolomite veins are cut by veins of clays, talc, and Fe-oxides as well as later calcite and aragonite veins. In one sample, dolomite appears to be partially overgrown by calcite.

Late-formed calcite veins clearly cross-cut earlier calcite veins and dolomite veins. Most are composed of grains (0.1–0.3 mm diameter) of radial crystal arrays. Others consist of more uniform crystals of similar grain size. Many late calcite veins line the walls of open fractures/cavities in the host troctolite or gabbro, often with a botryoidal surface appearance (Figure 4a). The fractures filled by late calcite veins are irregular and jagged in most samples, indicating formation under pure tension. Some veins are deposited in openings with arcuate, nonmatching walls, suggesting that the openings formed partially by dissolution of the host rock.

Aragonite veins typically consist of fibrous crystals oriented perpendicular to vein walls, equant crystals, or grains with radial growth patterns. Like many of the late-formed calcite veins, aragonite veins line the walls of open fractures. Most of the aragonite veins are either bounded by or intermixed with red-brown iron-(oxy)hydroxides (Figure 4c). Some of these iron-hydroxides also appear to consist of radial crystals with botryoidal surface appearances. It was not possible in most samples to establish a specific timing relationship between the formation of the late calcite veins and the aragonite veins, but in some cases aragonite veins overgrow earlier calcite veins.

Some aragonite veins also appear to grade in and out of sections of micrite-matrix breccia that fills tensile fractures in gabbro and troctolite (Figure 4d). The micrite breccias are matrix supported, and contain

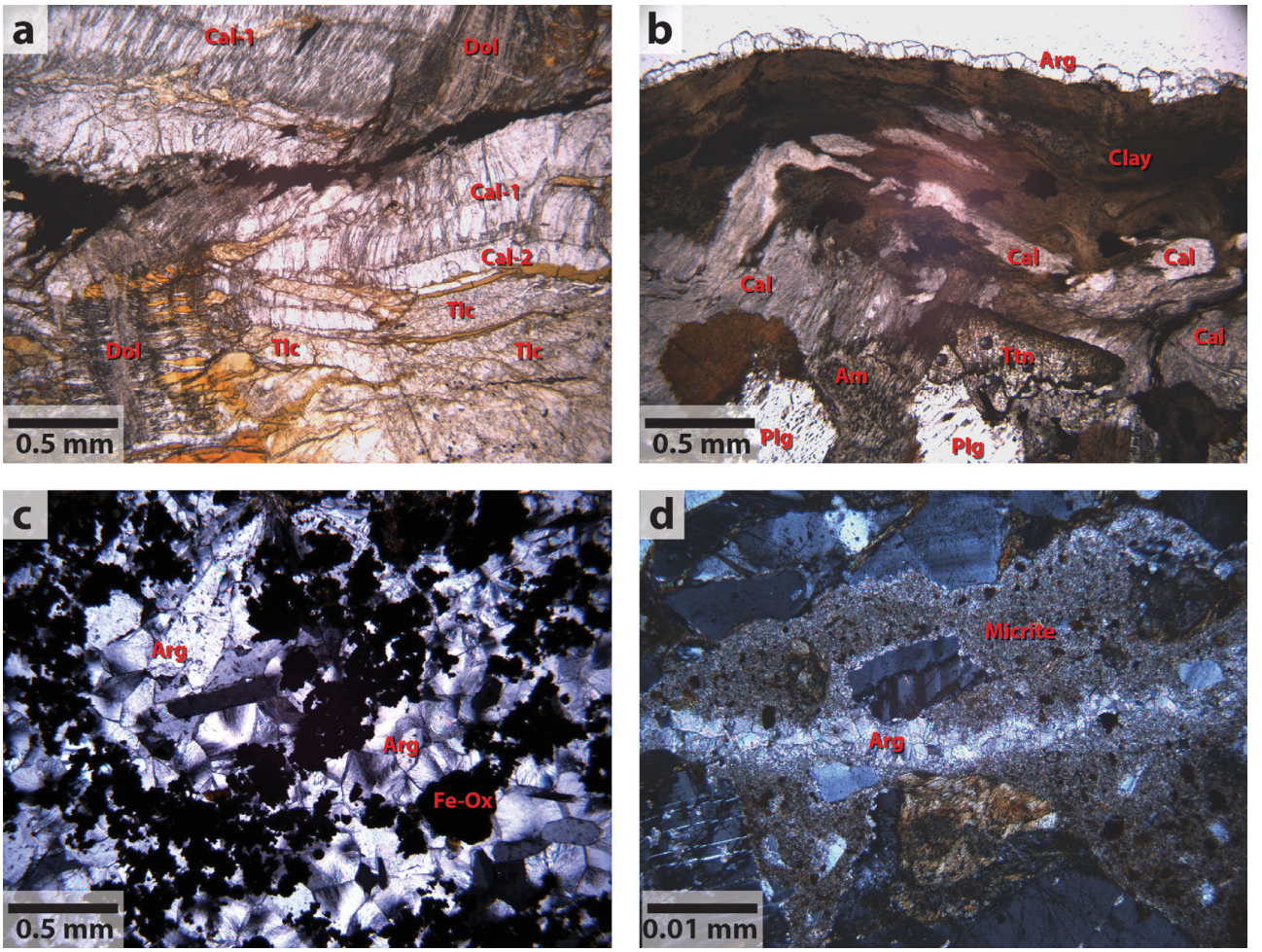

Figure 4. Photomicrographs. (a) Sample 1275D 10R-3 27–29 cm–Early dolomite vein in troctolite is offset by a microfault that has two generations of calcite veins precipitated along it; Dolomite vein contains numerous inclusions of small, unidentified phases; First generation of calcite veins (Cal-1) consists of fibrous crystals that bent with the microfault and was deformed with talc phacoids; second generation of calcite veins (Cal-2) fill tension fractures. (b) Sample 1275D 14R-1 2–6 cm–Calcite and aragonite veins in gabbro; early calcite veins are intermixed with amphibole and clay minerals within a shear zone; aragonite lines the margins of an open fracture in the rock. (c) Sample 1275D 25R-3 28–33 cm–Aragonite vein with iron hydroxides in troctolite. (d) Sample 1275B 6R-1 22–25 cm–Micrite-matrix breccia dikelet cutting diabase; aragonite vein with diffuse margins cuts down center of micrite; note that micrite matrix is partially recrystallized to coarser aragonite spar along vein margins. Mineral abbreviations: Am = Amphibole, Arg = aragonite, Cal = calcite, Dol = Dolomite, Fe-Ox = iron hydroxides, Pl = plagioclase, Ttn = titanite, Tlc = talc.

angular to sub-angular lithic and crystal fragments ranging in size from less than 0.1 mm to several mm in diameter. The breccia clasts represent all of the lithologies found at Site 1275. These breccias were likely formed by fluidized micrite being transported into fractures by infiltrating seawater. These micrite dikelets are cut by carbonate veins, around which some of the micrite has been recrystallized into coarse carbonate spar (Figure 4d). It is possible that some of the late veins are recrystallized biogenic micrite.

4. Methods

Samples used in this study were collected from core drilled during Ocean Drilling Program Leg 209 in 2003. Rock slabs were cut from the working half of the core both during the cruise and later at the MARUM repository. Shipboard logging data used in this study was downloaded from the JANUS database.

Carbonate material for isotopic analyses and solution elemental analyses was extracted from the drill-core slabs by microdrilling and sampling beneath a stereoscope. Care was taken to minimize sampling noncarbonate minerals in veins, minerals from noncarbonate veins, and the host rock. Drilled carbonate samples were then washed and centrifuged three times with ultra-pure water to remove all seawater salt and other impurities from the samples. Samples were then leached with 0.34 mmol ultra-pure acetic acid at room temperature.

The vials were then centrifuged and the supernate quantitatively transferred into PTFE beakers via pipet, before the acetic acid was evaporated at 110°C. One milliliter of 5.1 M HCl was then added to each beaker and evaporated until incipient dryness. This step was repeated three times. The wet precipitates were then dissolved in 200 μL 65% HNO_3 (sub-boiled) and 800 μL of ultra-pure water. The samples were heated in the closed PTFE beakers to 110°C for 5 h again before final dilution to a volume of 10 mL with ultra-pure water.

Major (Si, Al, Fe, Ca, Na, K, Mg, P) and trace elements (Ba, Sr) were analyzed in 10,000-fold dilution by inductively coupled plasma optical emission spectrometry using an Agilent 720 ICP-OES. Measured Ca concentrations were used to calculate the net sample weight assuming a conventional carbonate composition, whereas Si and Al concentrations were used to control for the amount of noncarbonates leached with this procedure.

Further trace element analyses were conducted in 10,000 times diluted aliquots at the Department of Geosciences, University of Bremen, Germany with a high-resolution inductively coupled plasma mass spectrometer (HR-ICP-MS, Element 2, Thermo Scientific) in low (Li, Rb, Y, Zr, Nb, Cs, Ba, light REE, Ta, Pb, Th, U), medium (Sc, V, Cr, Co, Ni, Cu, Zn, Ga) and high resolution (Hf, other REE) mode using indium as an internal standard. Accuracy and precision were checked with international reference material (JLS-1, CCH-1, BCR-2). Accuracy was better than 11% for all of the rare earth elements.

Oxygen and carbon isotopic compositions were measured on a Finnigan MAT-251 mass spectrometer at MARUM in Bremen, Germany. An internal standard of Solnhofen Limestone was used, which is calibrated against NBS 19. The long-term accuracy of this method ($\pm 2\,\sigma$) at MARUM is $<0.05‰$ for $\delta^{13}C$ and $<0.07‰$ for $\delta^{18}O$.

Strontium isotope ratios of carbonate samples were analyzed by thermal ionization mass spectrometry (TIMS) on a Triton plus instrument (Thermo Scientific) at the Isotope Chemistry Laboratory, Marum/Department of Geosciences, University of Bremen. Approximately 5 mg of carbonate were dissolved in HNO_3 at 75°C on the hotplate, dried, and redissolved in 500 μL of 2 M HNO_3 for chemical separation.

Strontium was isolated from the matrix elements by using miniaturized columns with 70 μL Sr.spec™. The separation procedure was adapted from *Deniel and Pin* [2001]. Total procedure blanks of Sr were <100 pg including a contribution of ~50 pg from the double distilled acids and are insignificant at the ~200 ng of sample-material that was used for analyses. Strontium was loaded in 0.1 M phosphoric acid with Ta-oxide emitter on Re single filaments and analyzed by TIMS in the dynamic multicollection mode. Instrumental mass-fractionation of Sr isotope ratios was normalized to $^{86}Sr/^{88}Sr$ of 0.1194. The external long-term reproducibility according to 200 ng loads of NIST 987 standard material is $^{87}Sr/^{86}Sr$ 0.710256 ± 16 (2σ, n=33; period: January 2013 to April 2014). The long-term reproducibility compares well with published values analyzed by TIMS of NIST 987 with an average of 0.710250 ± 32 (2SD, N=953, data <0.7102 and >0.7103 are discarded; GeoRem data base query May 2015; http://georem.mpch-mainz.gwdg.de)

In situ analyses of trace and major elements were carried out by laser-ablation ICP-MS at the Department of Geosciences, University of Bremen, using a NewWave UP193 solid-state laser coupled to an Element2 HR-ICP-MS). Carbonate analyses included Si and Al in order to detect possible contamination by minute silicate phases. Samples and standards were ablated with an irradiance of c. 1 $GWcm^{-2}$, spot sizes of 65 μm, and a laser pulse rate of 3 Hz. Plasma power was 1200 W, He (~0.8 $L{\cdot}min^{-1}$) was used as sample gas, and Argon (~0.8 $L{\cdot}min^{-1}$) was subsequently added as make-up gas. All isotopes were analyzed at low resolution with five samples in a 20% mass window and a total dwell time of 25 ms per isotope. Blanks were measured for 20 s prior to ablation. After every 8–12 samples NIST610 glass was analyzed as an external calibration standard using the values of *Jochum et al.* [2011]. For data quantification the Cetac GeoPro™ software was used with ^{43}Ca as internal standard (no interference with $^{27}Al^{16}O$ was observed). Data quality was assessed by analyses of USGS reference materials BCR2G, BHVO2G (basaltic glasses) and MACS-3 (carbonate) along with the samples (supporting information Data Set S1). External precision is better than 5% for most elements, accuracy as determined by comparison of our BCR2G and BHVO2G data with the GeoReM data base (as of January 2009) is better than 5% for most elements. Accuracy for MACS-3 is significantly worse (up to 20% for the REE), which we ascribe to a systematic deviation of the specimen used in the lab.

5. Results

5.1. Carbonate Vein Abundance

In order to assess the distribution and abundance of carbonate veins at Site 1275, we conducted an analysis of the vein log created by the metamorphic petrology group during Leg 209. We estimate the carbonate

fraction of recovered core from the vein log by multiplying the percentage of each core piece that was logged as carbonate vein by the length of that core piece, summing this result, and dividing by the sum of the piece lengths. The overall abundance of carbonate veins in Hole 1275D is approximately 0.15%. However, the veins are strongly concentrated in the troctolite sections of the core. Recovered troctolite is composed of 0.77% carbonate veins, while gabbroic rocks (including granophyre) are composed of only 0.01% carbonate veins. Percentage of carbonate veins binned into 5 meter intervals of curated depth (Figure 2) shows a strong correlation between carbonate vein abundance and the troctolite-dominated sections of the core in Hole 1275D. The vein log for Hole 1275B shows a significantly lower fraction of carbonate veins and no correlation with the troctolite. However, we examined a selection of cores in the MARUM archive and found that the shipboard log underestimates carbonate veins in Hole 1275B, particularly around the troctolite interval.

Estimates of carbonate abundance using geochemical analyses and thin sections suggest that significantly more carbonate exists in the troctolite, and to a lesser degree gabbro, than is apparent from veins visible in cut cores. We calculated the weight fraction of carbonate from the CO_2 volatile content analyzed as part of the shipboard geochemical suite (supporting information Data Set S2; Figure 2). These analyses indicate that the gabbroic sections are composed of 0.44 Wt.% carbonate minerals, and troctolite sections are 7.05 Wt.% carbonate minerals. These results are both significantly higher than estimates as suggested by the vein log, indicating a significant fraction of disseminated carbonate minerals and in veins that are too small to be easily observed in cut cores. Digitizing polygons over scanned thin sections revealed that some individual troctolite thin sections are composed of up to 15% carbonate minerals by volume, including veins and replacive calcite, consistent with the geochemical estimates.

5.2. Major and Trace Element Chemistry–Multiple Vein Populations

Elemental compositions from microdrilled veins and from thin-section laser-ablation analyses are presented in supporting information Data Sets S1 and S3 respectively, and selected results are shown graphically in Figure 5. Compositional fields of the microdrilled separate analyses and those of the laser-ablation generally overlap each other, indicating good agreement between the two analysis methods. Samples are grouped according to our textural classifications, and define distinct compositional fields. There is some degree of compositional overlap on the Mg versus Sr graph between early and late calcite veins (Figure 5a), as well as with the three analyses of replacive calcite. Early and late calcite vein populations are more distinct in Fe and Mn (Figure 5b).

Vein generations exhibit distinct rare earth element (REE) patterns. Aragonite veins have generally low REE content and negative cerium anomalies (Figure 5c), consistent with precipitation from oxidizing seawater. REE patterns are highly variable in calcite veins and replacive calcite. The early formed calcite veins generally have higher total REE content and high positive europium anomalies (Eu/Eu* up to +600; Figure 5d). Some of the late-formed calcite veins have similar REE profiles to the early veins, while others have similar patterns to the aragonite veins, i.e., lower overall REE contents, no europium anomalies, and/or negative cerium anomalies. This suggests precipitation from fluids that had varying degrees of interaction with the footwall rock. Dolomite veins are characterized by high REE content and strong positive Eu anomalies (Figure 5d).

It was difficult to analyze replacive calcite with the laser because of contamination by numerous fine silicate inclusions. Many analyses were discarded because of suspiciously high Si contents. Three of the better analyses (relatively low Si content) are included in this study (Figure 5d; supporting information Data Set S1). These have elemental concentrations most similar to the earlier formed calcite veins, with higher Mn and Fe content, and positive Eu anomalies. This is consistent with the textural relations between the replacive calcite and the early calcite veins, as well as the association between replacive calcite and talc.

Five of the six samples analyzed with laser-ablation ICP-MS contain multiple vein populations with distinct compositions and textures. Two representative samples, each with three vein populations, are shown in Figure 6 (1275D 10R-3 27–29 cm) and Figure 7 (1275D 6R-1 130 cm).

Sample 1275D 10R-3 27–29 cm (Figure 6) contains one generation of dolomite veins and two generations of calcite veins. The dolomite veins contain abundant small inclusions of silicate and oxide minerals and grade in and out of replacive calcite. The second calcite vein generation is fibrous and some of these veins

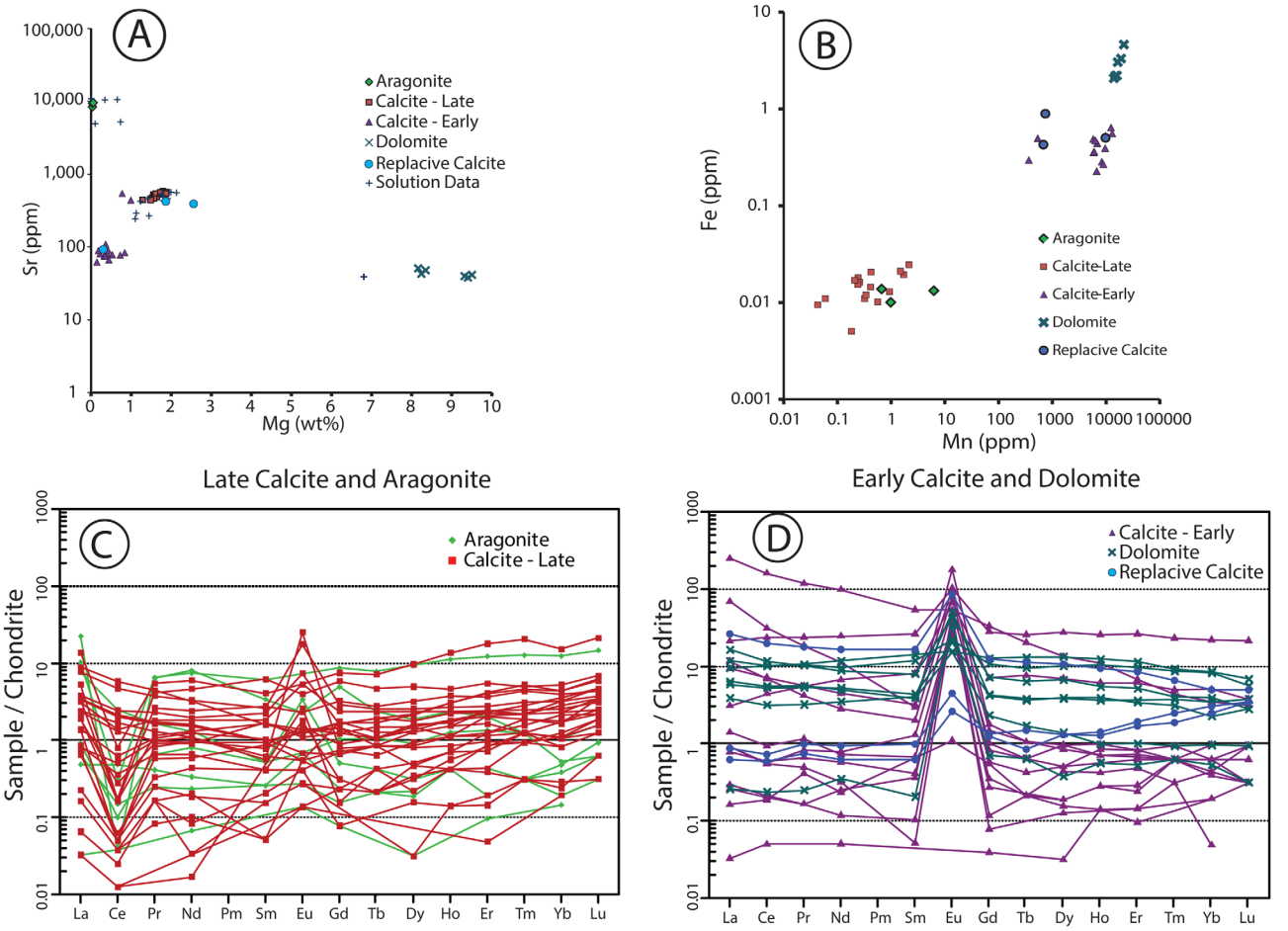

Figure 5. Vein carbonate compositions from microdrilled solution OES and laser-ablation-ICPMS analyses. (a) Plot of Mg versus Sr shows overlap between some overlap in compositions of early and late calcite veins. (b) Plot of Mn versus Fe shows overlap between aragonite and late calcite, but distinct compositions between two populations of early calcite and dolomite compositions. (c) REE compositions of aragonite and late calcite veins. (d) REE compositions of Early calcite and dolomite veins

are deformed with talc and clay minerals in a shear zone along the edge of the sample. The dolomite veins and first calcite veins have positive europium anomalies. The second generation of calcite veins clearly cuts both earlier vein generations and fills open cavities within the host troctolite. The late calcite veins have higher Sr content and negative Ce anomalies, indicating precipitation from oxidizing seawater. Also shown in the compositional plots for this sample is the solution ICP-MS analysis from the microdrilled sample, which consisted of a mixture of the two generations of calcite veins.

Sample 1275D 6R-1 130 cm (Figure 7) contains two generations of calcite veins and one generation of aragonite veins. The early (texturally determined) generation of calcite veins has relatively high Mg and Sr content, as well as a negative Ce anomaly and no Eu anomaly. These veins are cut by a later generation of calcite veins with lower Sr and Mg contents, higher overall REE content and a positive Eu anomaly, all indicating precipitation from fluids with higher temperature and a higher degree of bedrock interaction. The aragonite veins partially overgrow the first generation of calcite veins and have very low overall REE content, but a slight positive Eu anomaly.

5.3. Oxygen, Carbon, and Strontium Isotope Chemistry

Isotopic abundances are presented in supporting information Data Set S4. Oxygen isotopic compositions range from 34.5 to 36.0‰ $\delta^{18}O_{SMOW}$ for aragonite veins (n = 5) and from 11.0 to 36.5‰ $\delta^{18}O_{SMOW}$ for calcite veins (n = 18). Calculated precipitation temperatures for calcite and dolomite ranges from −8°C to 175°C (using formulation from *O'Neil* [1969]), and for aragonite from −4°C to −1°C (using formulation from

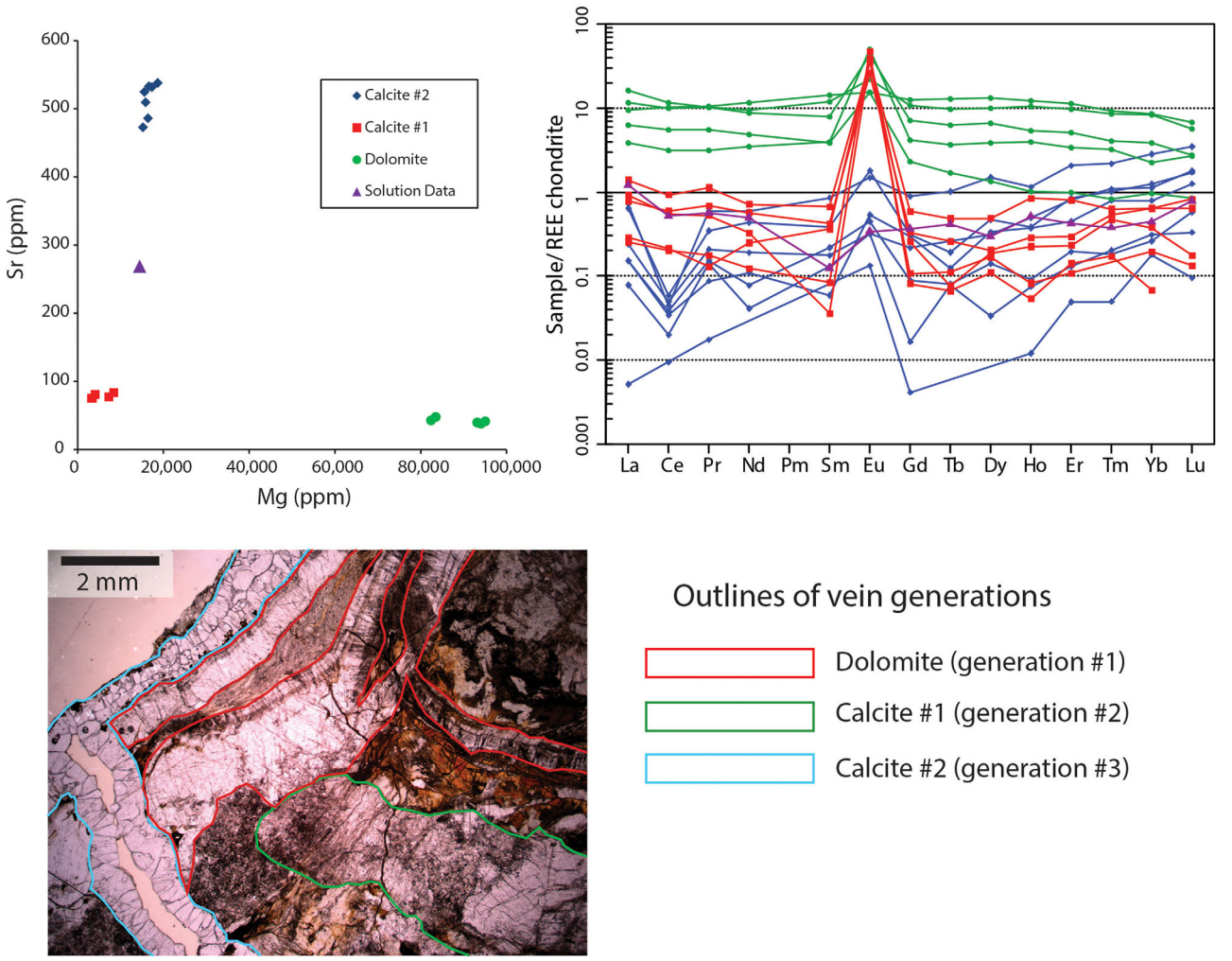

Figure 6. Compositions and photomicrographs of veins in Sample 1275D 10R-3 27–29 cm. Plot of Mg versus Ca clearly shows three vein generations–the microdrilled solution analysis lies between two vein populations, indicating that the separate included a composite of the two veins; The dolomite and first calcite veins have positive Eu anomalies, while the second calcite generation has a negative Ce anomaly.

Kim et al. [2007]). Temperature calculations were made using the composition of modern North Atlantic deep-sea water, 0.22‰ $\delta^{18}O_{SMOW}$ [*Shanks*, 2001]. Temperature estimates rise by approximately 6°C for low temperatures veins if a fluid composition of 1.5‰ $\delta^{18}O_{SMOW}$ is assumed for the veins. Temperatures slightly below 0°C (calculated from $\delta^{18}O_{SMOW}$ values greater than +36) are inconsistent with seafloor bottom temperatures at the time of precipitation. Similar results were obtained for several aragonite veins in nearby ODP Site 1271 [*Bach et al.*, 2011], and from serpentine-hosted aragonite veins at the nearby Logatchev hydrothermal vent field [*Eickmann et al.*, 2009]. Similar results were also reported for aragonite from the Lost City hydrothermal vent field [*Früh-Green et al.*, 2003]. These results could possibly be explained if seawater $\delta^{18}O$ was slightly higher than modern values, such as during a glacial maximum.

Carbon isotopic compositions range from −4.7 to +2.6‰ $\delta^{13}C_{PDB}$ in calcite and dolomite veins, and from +0.7 to +3.0‰ $\delta^{13}C_{PDB}$ in aragonite veins. These values are typical of seawater aragonites, and are similar to aragonite veins sampled nearby Site 1271 [*Bach et al.*, 2011] and the Logatchev vent field [*Eickmann et al.*, 2009]. Lower $\delta^{13}C$ values generally correlate lower $\delta^{18}O$ values and higher temperature of precipitation. $^{87}Sr/^{86}Sr$ ratios range from radiogenic seawater values 0.709207 to less radiogenic values of 0.704918, suggesting precipitation from fluids that had varying degrees of interaction with mafic rock.

Calcite veins that precipitated at high-temperatures also have high Mn & Fe contents, elevated REE's and strongly positive Eu anomalies. Calcite veins precipitated at lower temperature have lower Mn and Fe

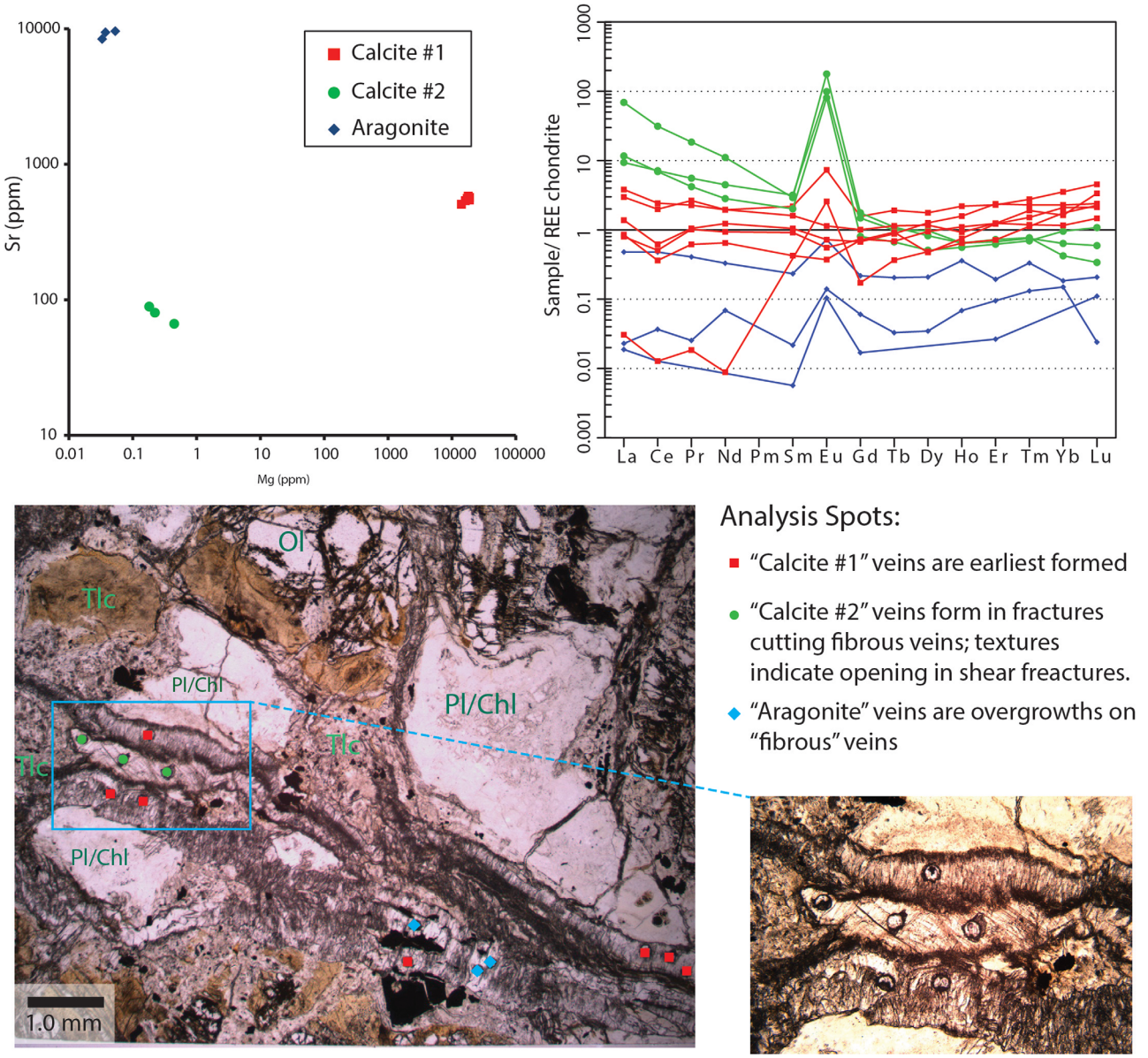

Figure 7. Compositions and photomicrographs of veins in Sample 1275D 6R-1 130–136 cm. The later "Calcite #2" veins have compositions indicative of precipitation from fluids with a higher degree of mafic-rock-interaction and at higher temperature than the earlier "Calcite #1" veins. This suggests alternating downward and upward fluid fluxing through fractures during unroofing of the detachment fault footwall.

contents, higher Mg and Sr content, and variable, but generally lower REE contents. Many low-temperature calcite veins also have negative Ce anomalies. Two microdrilled samples show compositional values that appear to be intermediate between the low-temperature veins and the higher-temperature veins (1275D-6R-1 130 cm and 1275D-10R-3 27–29 cm). Thin section inspection reveals that our microdrilling collected a composite of two vein generations. We reconstructed the isotopic compositions of the two vein components in Sample 1275D 10R-3 27–29 cm using the difference between its elemental composition analyzed via solution analysis and laser ablation. We determined that the separate used for solution and isotopic analyses was a mixture of 40% calcite from a low-temperature vein and 60% calcite from a high-temperature by using the ratio of the two laser compositions. We then estimated the high-temperature vein's isotopic composition by assuming that the low-temperature vein has similar isotopic composition to the other low-temperature veins (a seawater signature). This resulting estimate is consistent with the other analyses, and is included with the results in supporting information Data Set S4 and Figure 8.

6. Discussion

6.1. Seawater-Rock Interactions and Precipitation of Carbonates

The carbonate vein populations from Site 1275 core record multiple episodes of fluid movement through the detachment fault and likely also through secondary faults that cut the detachment. Our data indicate that carbonate precipitation in the footwall of an oceanic detachment fault can be triggered by multiple geochemical mechanisms and from many types of fluids. The oxygen and carbon isotopic signatures lie on a mixing line between Logatchev-like hydrothermal fluids and seawater (Figure 8a). We did not measure any veins with very high $\delta^{13}C$ values, such as the veins with $\delta^{13}C > +8$ found in nearby Site 1271 [*Bach et al*., 2011], which indicated abiogenic methane production at that site.

Though we were able to measure isotopic compositions of only a few high-temperature veins, these analyses allow us to draw correlations between vein compositions and textures. Our early formed veins precipitated at high temperatures, have elevated Mn and Fe contents, positive Eu anomalies, and lower $^{87}Sr/^{86}Sr$ (Figure 8b) than the late-formed veins. This is consistent with the early veins having precipitated from fluids that interacted with a higher volume of mafic rock at greenschist-grade temperatures. Our early veins have similar compositions to high-temperature calcite veins in talc-tremolite fault schists from the Logatchev hydrothermal vent field to the south of the 15°20′ FZ [*Eickmann et al*., 2009].

Estimated precipitation temperatures for the high-temperature veins are cooler than would be expected for an isenthalpic mixing of seawater and 400°C hydrothermal fluids (Figure 8b), suggesting that the upward transport of hydrothermal fluids through the fault(s) was slow enough to allow for conductive cooling. Similar slow transport was hypothesized for fluids precipitating high-temperature calcite veins from ODP Site 1271 [*Bach et al*., 2011] and to high-temperature calcite veins at the Logatchev hydrothermal field [*Eickmann et al*., 2009].

The strong correlation between the occurrence of high-temperature carbonate veins, replacive calcite, and troctolite suggests that the presence of olivine is a trigger for high-temperature carbonate precipitation. Alteration of olivine would drive down the fluids' oxygen fugacity and increase pH, thereby decreasing carbonate solubility [*Bonatti et al*., 1980]. The greater abundance of unaltered olivine near magmatic veins in troctolite may be the cause of higher carbonate occurrence. Talc and tremolite are also in locally higher abundance near magmatic veins (relative to serpentine dominated alteration away from the magmatic veins), and appear to be associated with carbonate precipitation. This schistose amphibole-talc assemblage is common in oceanic detachment faults [*Boschi et al*., 2006]. However, temperature estimates for the talc-tremolite assemblage are 270–350°C [*Boschi et al*., 2008], which is significantly warmer than our highest temperature calcite vein (174°C). Calcite in our samples appears to be more closely associated with talc than tremolite. It is possible that amphibole needles contained in calcite are a result of mechanical mixing of nonequilibrium assemblages. It is also possible that a talc-tremolite-calcite assemblage formed at higher temperatures, and then the oxygen isotopes were reset during later deformation of the veins.

We ran several reaction path models to predict stability conditions for the talc-calcite assemblage. The assemblage was most likely to precipitate at temperatures less than 200°C from fluids with low CO_2 and moderate SiO_2 activities. A model run with SiO_2 activity set at one log unit below quartz saturation (roughly the talc-serpentine equilibrium) predicts the assemblages magnesite -> talc-magnesite -> talc dolomite -> talc-calcite as aqueous CO_2 activity is decreased. Models run at lower silica activities predict serpentine-carbonate assemblages, which we observe in serpentinized parts of the troctolite, though in far less abundance than the calcite-talc assemblage near magmatic veins in troctolite.

An additional reaction path model run at 150°C and 1 kbar predicts the assemblages that would develop in troctolite fluxed with slightly CO_2-enriched seawater-derived fluids. Figure 9 plots the volume of minerals that are predicted to form against the mass of troctolite titrated into 1 kg of fluid. The talc-calcite assemblage is predicted to be dominant at highest water-to-rock ratios, and serpentine becomes the primary phase as the volume of troctolite rock in the mixture is increased. These results suggest that the variations in alteration mineral assemblage may be due to local variations in the degree of fluid fluxing and rock interaction. Carbonate mineralization occurs most prominently near gabbroic/magmatic veins in troctolite. This could be due to metasomatic compositional variations near the magmatic veins and/or enhanced fluid flow along the veins. Our modeling supports the idea that higher water to rock ratios (i.e., higher fluid fluxing)

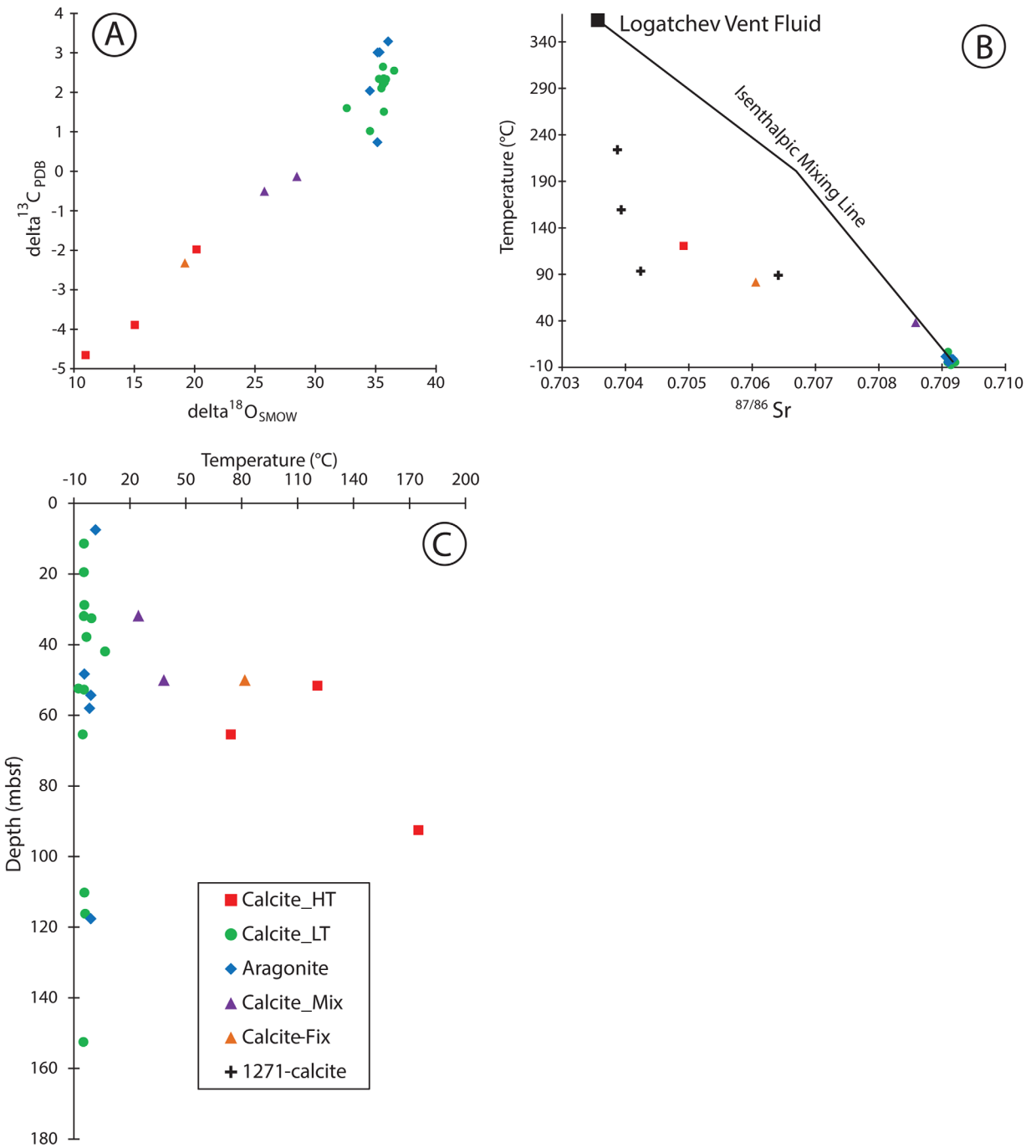

Figure 8. Graphs of isotope data–plots include two data points that were physical mixes of two separate vein compositions (Calcite-Mix), and one data point that is one of mixed sample's isotopic compositions corrected to the high-temperature calcite using solution and laser ablation trace element analyses (Calcite-Fix; see text for method). (a) Oxygen versus Carbon isotopes appear to lie on a mixing line between a Logatchev-like hydrothermal fluid and seawater. (b) Temperature from oxygen isotopes versus Strontium isotopes, analyzes of calcite veins from Site 1271 [*Bach et al*., 2011] included–vein compositions plot at lower temperatures than a mixing line between sweater and a Logatchev-like hydrothermal fluids indicating conductive cooling during ascent. (c) Graph of temperature from oxygen isotopes versus depth below sea floor–no trend is apparent

could promote the calcite-talc assemblage, but does not rule out the possibility that compositional effects also are important.

6.2. Carbonate Veins and Detachment Faulting

Prior work by *Schroeder et al*. [2007] suggests that strain localization on the 15°45′ detachment fault was initiated at middle- to upper-amphibolite facies conditions (600–750°C) during intrusion of late-stage diabase.

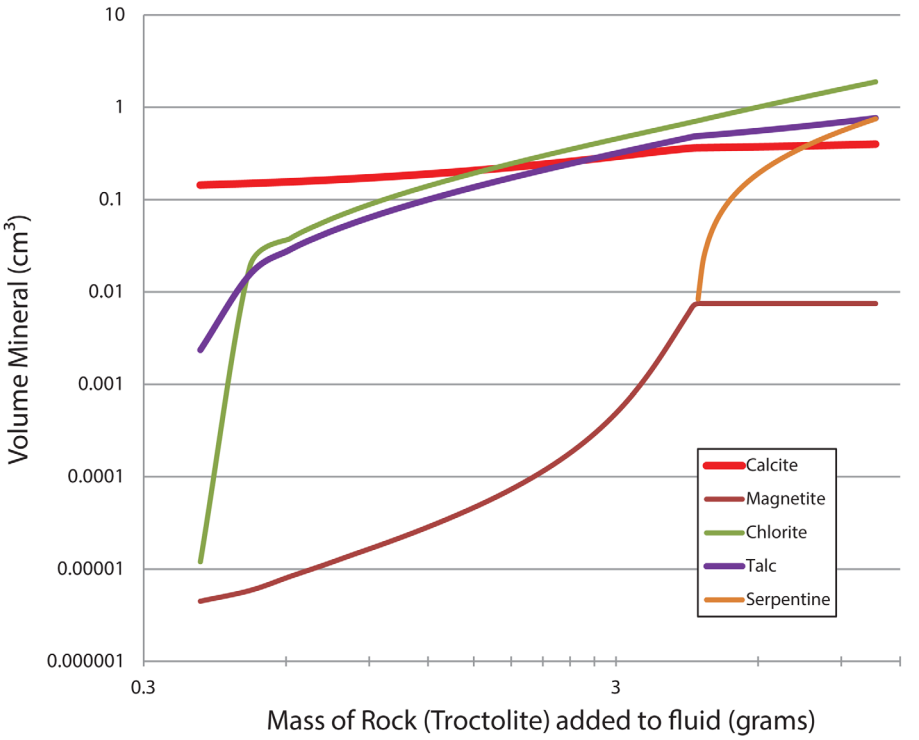

Figure 9. Output at reaction path model run to predict stability conditions of the talc-calcite assemblage in troctolite; model run at 150°C and 1 kbar fluxed with slightly CO_2-enriched seawater-derived fluids; predicts stability of assemblage at high water-rock ratios, and increasing abundance of serpentine as additional troctolite is titrated into fluid.

Detachment faulting continued to greenschist-grade-temperatures associated with the formation of tremolite-talc-chlorite schists that cut earlier high-temperature shear zones, some of which include deformed calcite.

The general trend of vein crosscutting relations is for higher temperature veins to be cut by lower-temperature veins, as would be expected in an extensional fault footwall. This trend, however, is not true in sample 1275D-6R-1 130–136 cm, in which a low-temperaure calcite vein is cut by a high-temperature calcite vein (Figure 7). This indicates that the fluid regime in the fault did not evolve in a simple down-temperature fashion during footwall denudation. Instead it alternated from being dominated by seawater and upwelling hydrothermal fluids, which may represent variations of fluid mixing in the fault zone. Upward pulsing of hydrothermal fluids could be triggered by a deformation-induced porosity changes, or by dike injection deeper within the fault, either of which could have increased the hydrothermal fraction of the fluid mix.

There is no systematic relationship between depth within the holes and the temperature of carbonate vein precipitation (Figure 8c), and veins that precipitated at seawater temperatures appear >150 mbsf depth. This indication of an effectively zero shallow geothermal gradient is different than the 100–150°C km^{-1} gradient recorded by carbonate veins at nearby ODP Site 1274 [*Bach et al*., 2011]. This is also different than the gabbroic footwall of Atlantis Massif OCC (30°N, MAR), where borehole logging in IODP Hole 1309D [*Ildefonse*, 2005; *Blackman et al*., 2014] indicate a geothermal gradient of ~100°C km^{-1} at this depth range. Carbonate vein precipitation temperatures (estimated from oxygen isotopes) of the coolest-precipitated veins at each depth in Hole 1309D [*Jöns et al*., 2013] are consistent with the pore water temperature measurements. It is difficult to make direct comparisons between these sites, as the 15°45′ Core Complex is several million years further off-axis than the other two. However, seawater-temperature veins at depth in Hole 1275D suggest that either footwall of the 15°45′ Core Complex was very effectively cooled by water circulation during faulting, or that carbonate vein precipitation continued long after footwall denudation and cooling.

6.3. Carbonate Veins as a CO_2 Sink

Shipboard measurement in Site 1275 cores indicate that ~0.15% of the rock volume is carbonate veins, corresponding to a weight fraction of ~0.075% CO_2. This is roughly similar to the 0.1% CO_2 uptake by

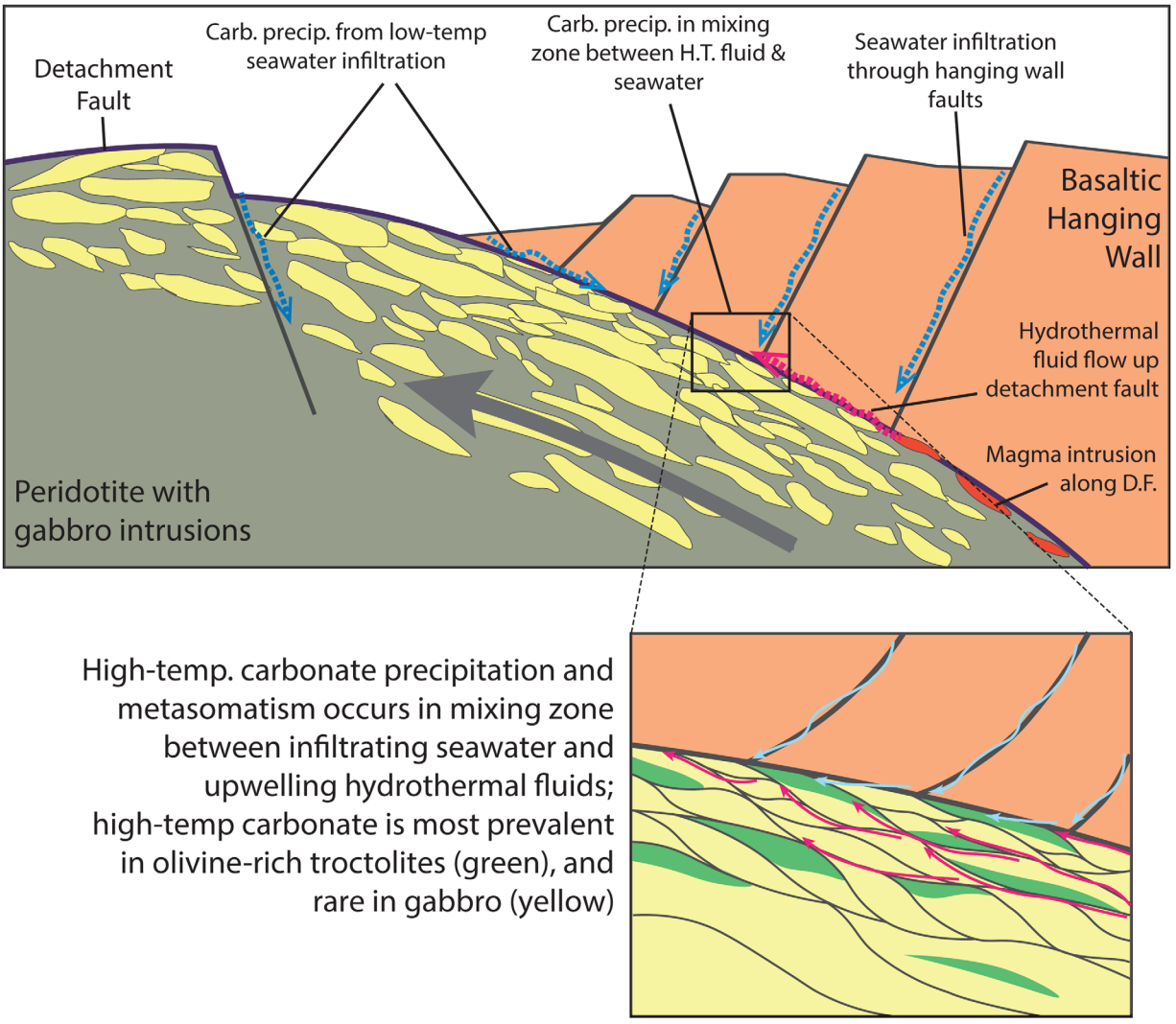

Figure 10. Schematic cross section depicting fluid mixing and carbonate precipitation in core complex footwall; hydrothermal fluids derive from greenschist alteration and possibly magmatic fluids deep within the footwall; Inset shows mixing of hydrothermal fluids at higher levels of the anastomosing fault zone–carbonate precipitation is most prominent in troctolite enclaves.

aragonite veins measured in the serpentinized peridotite core from nearby ODP Sites 1271 and 1274 [*Bach et al*., 2011]. This estimate is also similar to gabbroic core at ODP Site 735 on the Southwest Indian Ridge [*Bach et al*., 2001], modern serpentinite cores at other sites in the Atlantic [*Alt et al*., 2013], and slightly lower than modern volcanic rocks from Atlantic crust [*Gillis and Coogan*, 2011]. This estimate of CO_2 uptake is significantly less than the estimated 2–3% CO_2 uptake in Cretaceous and Jurassic volcanic oceanic crust [*Staudigel et al*., 1996; *Alt and Teagle*, 1999, *Gillis and Coogan*, 2011]. Greater carbonate precipitation in oceanic crust during the Mesozoic was likely due to differences in seawater chemistry at the time [*Gillis and Coogan*, 2011]. .

The much higher abundance of carbonate veins and carbonated olivine observed in troctolite sections of Site 1275 core are interesting from the perspective of proposals to use ophiolitic peridotite for carbon dioxide sequestration [i.e., *Kelemen and Matter*, 2008; *Power et al*., 2013]. The average CO_2 uptake by troctolite sections of the holes is estimated to be 0.4% from the vein log, and 3.0% from geochemical analyses and thin section quantification, which take into account disseminated and replacive calcite. These values are much higher than have been found at any other studied locations in modern oceanic lithosphere [*Gillis and Coogan*, 2011; *Alt et al*., 2013]. The conditions that appear to be most conducive to carbonate precipitation are fluid-rock interactions with nonserpentinized olivine and high water-to-rock ratios at ~150°C. These

observations may be important while considering engineered CO_2 sequestration via olivine carbonation. Efforts to date have focused on the serpentine-to-magnesite reaction, while our observations indicate that an olivine-to-calcite reaction could also be effective.

7. Conclusions

Carbonate precipitated within the Site 1275 detachment fault from a mixture of infiltrating seawater with high-temperature hydrothermal fluids. The fluid-mixing regime in the fault (Figure 10) did not result in a simple down-temperature mineral precipitation path, but alternated from being dominated by high-temperature fluids and low-temperature seawater. Multiple fluids utilized similar pathways, as up to three distinct generations of carbonate veins are present within the space of a single thin section. Thus, temperature estimates obtained from minerals in detachment faults may be more representative of ephemeral fluid conditions than the temperatures of the surrounding rock. However, it is uncertain how quickly these might change, as our precipitation temperature estimates are cooler than a simple iso-enthalpic mixing between seawater and a 400°C hydrothermal fluid, suggesting that flow was slow enough to allow for conductive cooling. Highest degrees of carbonate precipitation occurred in samples in which large volumes of 100–150°C fluids interacted with nonserpentinized olivine in troctolite (Figure 10). The last-formed, low-temperature calcite and aragonite veins likely formed under more oxidizing, seawater-dominated conditions, possibly associated with secondary faults that cut the detachment following footwall denudation. The lack of a systematic depth-temperature relationship and the presence of seawater-temperature veins at >150 mbsf depths in the hole indicate that active seawater infiltration effectively cooled the detachment during or post denudation.

Acknowledgments

Whole rock geochemical data used to estimate carbonate fraction of samples was unpublished data compiled by Holger Paulick [*Paulick et al*., 2006]. This data is included in the supporting information. Several of the carbonate isotope and major element analyses used in this study are unpublished data generated by Martin Rosner, and are indicated as such in the supporting information. This work was supported by a fellowship from the Hanse-Wissenschaftskolleg in Delmenhorst, Germany, and by grant funding from MARUM Bremen, Germany. Samples were collected from the IODP Bremen Core Repository at MARUM under IODP sample request 22959B.

References

Alt, J. C., and D. A. H. Teagle (1999), The uptake of carbon during alteration of ocean crust, *Geochim. Cosmochim. Acta*, *63*(10), 1527–1535.

Alt, J. C., and D. A. H. Teagle (2003), Hydrothermal alteration of upper oceanic crust formed at a fast-spreading ridge: Mineral, chemical, and isotopic evidence from ODP Site 801, *Chem. Geol.*, *201*(3-4), 191–211, doi:10.1016/S0009-2541(03)00201-8.

Alt, J. C., E. M. Schwarzenbach, G. L. Früh-Green, W. C. Shanks III, S. M. Bernasconi, C. J. Garrido, L. Crispini, L. Gaggero, J. A. Padrón-Navarta, and C. Marchesi (2013), The role of serpentinites in cycling of carbon and sulfur: Seafloor serpentinization and subduction metamorphism, *Lithos*, *178*, 40–54, doi:10.1016/j.lithos.2012.12.006

Bach, W., J. C. Alt, Y. Niu, S. E. Humphris, J. Erzinger, and H. J. B. Dick (2001), The geochemical consequences of late-stage low-grade alteration of lower ocean crust at the SW Indian Ridge: Results from ODP Hole 735B (Leg 176), *Geochim. Cosmochim. Acta*, *65*(19), 3267–3287, doi:10.1016/S0016-7037(01)00677-9.

Bach, W., B. Peucker-Ehrenbrink, S. R. Hart, and J. S. Blusztajn (2003), Geochemistry of hydrothermally altered oceanic crust: DSDP/ODP Hole 504B–Implications for seawater-crust exchange budgets and Sr- and Pb-isotopic evolution of the mantle, *Geochem. Geophys. Geosyst.*, *4*(3), 8904, doi:10.1029/2002GC000419.

Bach, W., C. J. Garrido, H. Paulick, J. Harvey, and M. Rosner (2004), Seawater-peridotite interactions: First insights from ODP Leg 209, MAR 15°N, *Geochem. Geophys. Geosyst.*, *5*, *Q09F26*, doi:10.1029/2004GC000744.

Bach, W., M. Rosner, N. Jöns, S. Rausch, L. F. Robinson, H. Paulick, and J. Erzinger (2011), Carbonate veins trace seawater circulation during exhumation and uplift of mantle rock: Results from ODP Leg 209, *Earth Planet. Sci. Lett.*, *311*(3-4), 242–252, doi:10.1016/j.epsl.2011.09.021.

Blackman, D. K., A. Slagle, G. Guerin, and A. Harding (2014), Geophysical signatures of past and present hydration within a young oceanic core complex, *Geophys. Res. Lett.*, *41*, 1179–1186, doi:10.1002/2013GL058111.

Bonatti, E., J. R. Lawrence, P. R. Hamlyn, and D. Breger (1980), Aragonite from deep sea ultramafic rocks, *Geochim. Cosmochim. Acta*, *44*(8), 1207–1214, doi:10.1016/0016-7037(80)90074-5.

Boschi, C., G. L. Früh-Green, and J. Escartín (2006), Occurrence and significance of serpentinite-hosted, talc- and amphibole-rich fault rocks in modern oceanic settings and ophiolite complexes: An overview, *Ofioliti*, *31*(2), 129–140, doi:10.4454/ofioliti.v31i2.335.

Boschi, C., A. Dini, G. L. Früh-Green, and D. S. Kelley (2008), Isotopic and element exchange during serpentinization and metasomatism at the Atlantis Massif (MAR 30°N): Insights from B and Sr isotope data, *Geochim. Cosmochim. Acta*, *72*(7), 1801–1823, doi:10.1016/j.gca.2008.01.013.

Buck, W. R., L. L. Lavier, and A. N. B. Poliakov (2005), Modes of faulting at mid-ocean ridges., *Nature*, *434*(7034), 719–23, doi:10.1038/nature03358.

Cann, J. R., D. K. Blackman, D. K. Smith, E. McAllister, B. Janssen, S. Mello, E. Avgerinos, A. R. Pascoe, and J. Escartin (1997), Corrugated slip surfaces formed at ridge–transform intersections on the Mid-Atlantic Ridge, *Nature*, *385*(6614), 329–332, doi:10.1038/385329a0.

Cannat, M. (1993), Emplacement of mantle rocks in the seafloor at mid-ocean ridges, *J. Geophys. Res.*, *98*(B3), 4163–4172, doi:10.1029/92JB02221.

Cannat, M., Y. Lagabrielle, and H. Bougault (1997), Ultramafic and gabbroic exposures at the Mid-Atlantic Ridge: Geological mapping in the 15°N region, *Tectonophysics*, *279*, 193–213.

Coggon, R. M., D. A. . Teagle, M. J. Cooper, and D. A. Vanko (2004), Linking basement carbonate vein compositions to porewater geochemistry across the eastern flank of the Juan de Fuca Ridge, ODP Leg 168, *Earth Planet. Sci. Lett.*, *219*(1-2), 111–128, doi:10.1016/S0012-821X(03)00697-6.

Coggon, R. M., D. A. H. Teagle, C. E. Smith-Duque, J. C. Alt, and M. J. Cooper (2010), Reconstructing past seawater Mg/Ca and Sr/Ca from mid-ocean ridge flank calcium carbonate veins, *Science*, *327*(5969), 1114–7, doi:10.1126/science.1182252.

Deniel, C., and C. Pin (2001), Single-stage method for the simultaneous isolation of lead and strontium from silicate samples for isotopic measurements, *Anal. Chim. Acta*, *426*(1), 95–103, doi:10.1016/S0003-2670(00)01185-5.

Eickmann, B., W. Bach, M. Rosner, and J. Peckmann (2009), Geochemical constraints on the modes of carbonate precipitation in peridotites from the Logatchev Hydrothermal Vent Field and Gakkel Ridge, *Chem. Geol.*, *268*(1-2), 97–106, doi:10.1016/j.chemgeo.2009.08.002.

Elderfield, H., and A. Schultz (1996), Mid-ocean ridge hydrothermal fluxes and the chemical composition of the ocean, *Annu. Rev. Earth Planet. Sci.*, *24*(1), 191–224, doi:10.1146/annurev.earth.24.1.191.

Escartín, J., and M. Cannat (1999), Ultramafic exposures and the gravity signature of the lithosphere near the Fifteen–Twenty Fracture Zone (Mid-Atlantic Ridge, 14°–16.5°N), *Earth Planet. Sci. Lett., 171*, *411–424.*

Escartín, J., C. Mével, C. J. MacLeod, and A. M. McCaig (2003), Constraints on deformation conditions and the origin of oceanic detachments: The Mid-Atlantic Ridge core complex at 15°45′N, *Geochem. Geophys. Geosyst.*, *4*(8), 1067, doi:10.1029/2002GC000472.

Früh-Green, G. L., D. S. Kelley, S. M. Bernasconi, J. A. Karson, K. A. Ludwig, D. A. Butterfield, C. Boschi, and G. Proskurowski (2003), 30,000 years of hydrothermal activity at the lost city vent field., *Science*, *301*(5632), 495–8, doi:10.1126/science.1085582.

Fujiwara, T., J. Lin, T. Matsumoto, P. B. Kelemen, B. E. Tucholke, and J. F. Casey (2003), Crustal Evolution of the Mid-Atlantic Ridge near the Fifteen-Twenty Fracture Zone in the last 5 Ma, *Geochem. Geophys. Geosyst.*, *4*(3), 1024, doi:10.1029/2002GC000364.

Garcés, M., and J. S. Gee (2007), Paleomagnetic evidence of large footwall rotations associated with low-angle faults at the Mid-Atlantic Ridge, *Geology*, *35*(3), 279, doi:10.1130/G23165A.1.

Gillis, K. M., and L. A. Coogan (2011), Secular variation in carbon uptake into the ocean crust, *Earth Planet. Sci. Lett.*, *302*(3-4), 385–392, doi:10.1016/j.epsl.2010.12.030.

Ildefonse, B. (2005), IODP Expeditions 304 and 305: Oceanic Core Complex Formation, Atlantis Massif, *Sci. Drill.*, *1*(1), 28–31, doi:10.5194/sd-1-28-2005.

Jochum, K. P., et al. (2011), Determination of reference values for NIST SRM 610-617 glasses following ISO guidelines, *Geostand. Geoanal. Res.*, *35*(4), 397–429, doi:10.1111/j.1751-908X.2011.00120.x.

Jöns, N., W. Bach, M. Rosner, and B. Plessen (2013), Formation of late-stage mineral veins in the footwall of an oceanic detachment fault (ODP Leg 304/305), Abstract EGU2013-5457 presented at General Assembly 2013, EGU, Vienna.

Kelemen, P. B., and J. Matter (2008), In situ carbonation of peridotite for CO2 storage, *Proc. Natl. Acad. Sci. U. S. A.*, *105*(45), 17,295–17,300, doi:10.1073/pnas.0805794105.

Kelemen, P. B., et al. (2004), *Volume 209 Initial Reports*, 1st ed., Ocean Drill. Program, College Station, Tex.

Kim, S.-T., J. R. O'Neil, C. Hillaire-Marcel, and A. Mucci (2007), Oxygen isotope fractionation between synthetic aragonite and water: Influence of temperature and Mg2+ concentration, *Geochim. Cosmochim. Acta*, *71*(19), 4704–4715, doi:10.1016/j.gca.2007.04.019.

Macleod, C. J., J. Escartín, D. Banerji, G. J. Banks, M. Gleeson, D. H. B. Irving, R. M. Lilly, A. M. Mccaig, S. Allerton, and D. K. Smith (2002), Direct geological evidence for oceanic detachment faulting: The Mid-Atlantic Ridge, 15°45′N, *Geology*, *30*(10), 879–882, doi:10.1130/0091-7613(2002)030<0879.

MacLeod, C. J., J. Carlut, J. Escartín, H. Horen, and A. Morris (2011), Quantitative constraint on footwall rotations at the 15°45′N oceanic core complex, Mid-Atlantic Ridge: Implications for oceanic detachment fault processes, *Geochem. Geophys. Geosyst.*, *12*, Q0AG03, doi:10.1029/2011GC003503.

Mottl, M. J., and C. G. Wheat (1994), Hydrothermal circulation through mid-ocean ridge flanks: Fluxes of heat and magnesium, *Geochim. Cosmochim. Acta*, *58*(10), 2225–2237, doi:10.1016/0016-7037(94)90007-8.

O'Neil, J. R. (1969), Oxygen Isotope Fractionation in Divalent Metal Carbonates, *J. Chem. Phys.*, *51*(12), 5547, doi:10.1063/1.1671982.

Paulick, H., W. Bach, M. Godard, J. C. M. De Hoog, G. Suhr, and J. Harvey (2006), Geochemistry of abyssal peridotites (Mid-Atlantic Ridge, 15°20′N, ODP Leg 209): Implications for fluid/rock interaction in slow spreading environments, *Chem. Geol.*, *234*(3-4), 179–210, doi:10.1016/j.chemgeo.2006.04.011.

Power, I. M., A. L. Harrison, G. M. Dipple, S. A. Wilson, P. B. Kelemen, M. Hitch, and G. Southam (2013), Carbon Mineralization: From Natural Analogues to Engineered Systems, *Rev. Mineral. Geochem.*, *77*(1), 305–360, doi:10.2138/rmg.2013.77.9.

Rona, P. A., L. Widenfalk, and K. Boström (1987), Serpentinized ultramafics and hydrothermal activity at the Mid-Atlantic Ridge crest near 15°N, *J. Geophys. Res.*, *92*(B2), 1417–1427, doi:10.1029/JB092iB02p01417.

Schroeder, T., M. J. Cheadle, H. J. B. Dick, U. Faul, J. F. Casey, and P. B. Kelemen (2007), Nonvolcanic seafloor spreading and corner-flow rotation accommodated by extensional faulting at 15°N on the Mid-Atlantic Ridge: A structural synthesis of ODP Leg 209, *Geochem. Geophys. Geosyst.*, *8*, *Q06015*, doi:10.1029/2006GC001567.

Shanks, W. C. (2001), Stable Isotopes in Seafloor Hydrothermal Systems: Vent fluids, hydrothermal deposits, hydrothermal alteration, and microbial processes, *Rev. Mineral. Geochem.*, *43*(1), 469–525, doi:10.2138/gsrmg.43.1.469.

Staudigel, H., T. Plank, W. White, and H. U. Schmincke (1996), Geochemical fluxes during seafloor alteration of the basaltic oceanic crust: DSDP Sites 417-418 (Overview), in *Subduction Top to Bottom*, edited by G. E. Bebout et al., pp. 19–38, AGU, Washington, D. C.

Teagle, D. A. H., M. J. Bickle, and J. C. Alt (2003), Recharge flux to ocean-ridge black smoker systems: A geochemical estimate from ODP Hole 504B, *Earth Planet. Sci. Lett.*, *210*(1-2), 81–89, doi:10.1016/S0012-821X(03)00126-2.

Tucholke, B. E., and J. Lin (1994), A geological model for the structure of ridge segments in slow spreading ocean crust, *J. Geophys. Res.*, *99*(B6), 11,937-11,958, doi:10.1029/94JB00338.

Tucholke, B. E., M. D. Behn, W. R. Buck, and J. Lin (2008), Role of melt supply in oceanic detachment faulting and formation of megamullions, *Geology*, *36*(6), 455, doi:10.1130/G24639A.1.

Wheat, C. G., and M. J. Mottl (2000), Composition of pore and spring waters from Baby Bare: Global implications of geochemical fluxes from a ridge flank hydrothermal system, *Geochim. Cosmochim. Acta*, *64*(4), 629–642, doi:10.1016/S0016-7037(99)00347-6.